Regular Article

PHYSICAL CHEMISTRY RESEARCH
Published by the
Iranian Chemical Society
www.physchemres.org
info@physchemres.org

Phys. Chem. Res., Vol. 9, No. 2, 327-344, June 2021
DOI: 10.22036/pcr.2021.246397.1825

Using Iron-copper Nanocomposites Prepared by Peanut Vine Extracts for the Removal of Pefloxacin and Enrofloxacin from an Aqueous Solution: Isotherms, Kinetics, and Mechanism

Y.Y. Niu[a], X.L. Han[a,b,*], L.L. Liang[a], C. Chang[a,b] and J.Y. Chen[a,b]

[a]*School of Chemical Engineering, Zhengzhou University, Zhengzhou 450001, China*
[b]*Henan Outstanding Foreign Scientists' Workroom, Zhengzhou 450001, China*

(Received 2 September 2020, Accepted 28 February 2021)

Herein, A facile and green approach was employed to fabricate iron-copper nanocomposites (ICNCs) using peanut vine extracts, and the ICNCs were used for the removal of pefloxacin (PFX) and enrofloxacin (ENR) from an aqueous solution. Following this, ICNCs were comprehensively characterized by BET, XPS, SEM, FT-IR and EDS. The equilibrium adsorption data of PFX and ENR on ICNCs were well described by Langmuir and Sips isotherm models, and thermodynamics parameters revealed the spontaneous and endothermic nature of PFX and ENR adsorption processes. Kinetic data were best fitted by pseudo-second-order model. Hydrogen bonding, π-π and n-π electron-donor-acceptor interaction, complexation and electrostatic interaction were the main forces in the adsorption process of ICNCs. The maximum monolayer adsorption capacities of ICNCs for PFX and ENR were 240.70 and 195.97 mg g^{-1} at 298 K, respectively, indicating that ICNCs is a promising adsorbent for PFX or ENR removal in wastewater treatment.

Keyword: Adsorption, Iron-copper nanocomposites, Peanut vine, Pefloxacin, Enrofloxacin

INTRODUCTION

A great number of poorly metabolic antibiotics are only excreted by humans or animals and directly entered natural water bodies [1,2]. Low concentrations of antibiotics left in the environment constitute rising intimidation to mankind health and ecology, *via* promoting the growth of antibiotic-resistant bacteria and disturbing ecological equilibrium [2,3]. Pefloxacin and enrofloxacin are representative drugs among quinolones antibiotics that have been detected in water all over the world [4]. Therefore, how to remove pefloxacin and enrofloxacin from aquatic environments has become more and more urgent.

In recent years, several methods such as biological treatment, ion-exchange, advanced oxidation techniques, adsorption, photolysis and electrochemical decomposition have been proposed to treat the wastewater of pefloxacin and enrofloxacin by researchers [5-12]. These methods have disadvantages, for instance, advanced oxidation techniques often cause energy intensive, and activated sludge may render the increasing toxicity of wastewater [12,13]. Compared with other treatment mediums, adsorption was the most promising method because it is low-cost, eco-friendly and easily operated. Halloysite nanotubes, Fe-Mn modified biochar using vinasse wastes, and oxidized multiwalled carbon nanotubes were used to adsorb pefloxacin from wastewater [1,7,14]. Enrofloxacin was removed from aqueous solutions by activated carbon prepared from industrial paper sludge, clay minerals and Na-montmorillonite [15-17]. Among all adsorbents, nano-sized materials have been received substantial attention due to their stable morphology and large specific surface [18]. Whereas, the methods for the synthesis of nanomaterials have disadvantages such as complex operation, high price and the use of hazardous reagents [19]. Accordingly, it is of necessity to develop a green, simple and sustainable

*Corresponding author. E-mail: xlhan@zzu.edu.cn

approach to synthesize nanoadsorbents.

Nowadays, the synthesis of metal-based nanomaterials by plant extracts has become more attractive. Plant extracts were applied as reducing agent instead of organic solvents and chemical compounds in this method [19]. They are rich in polyphenolic [20] and flavonoid [21,22], which were used as reducing and capping agents [23]. The metal ions, reduced initially, result in the formation of nucleation centers, then the nucleation centers seclude extra metal ions and involve adjacent nucleation sites, ultimately leading to the formation of nanoadsorbents [24]. Moreover, it has also been reported that this method is non-toxic and greener than traditional chemical reagents for preparing metal-based nanomaterials [25,26].

In this study, ICNCs were synthesized by peanut vine extracts for the removal of pefloxacin and enrofloxacin from wastewater. Furthermore, the adsorption characterizations of pefloxacin and enrofloxacin on ICNCs were investigated.

EXPERIMENTAL

Materials and Chemicals

The following chemical reagents were used in this paper: Ferric chloride hexahydrate ($FeCl_3 \cdot 6H_2O$) and cupric chloride dihydrate ($CuCl_2 \cdot 2H_2O$) were both bought from Sinopharm Chemical Reagent Co. Ltd. Pefloxacin (PFX, $C_{18}H_{28}FN_3O_8S$, ≥99%) was received from Daming Biotech. Co. Ltd. Enrofloxacin hydrochloride (ENR, $C_{19}H_{23}ClFN_3O_3$, ≥98%) was purchased from MedChem Express, Shanghai, China. Peanut vines were collected from Xinxiang, China. The PFX and ENR stock solution (1 g l^{-1}) were prepared with deionized water and reposited in the refrigerator.

Preparation of Peanut Vine Extracts

The peanut vines were thoroughly pre-washed three times by deionized water in order to eliminate dirt and dried at 325 K until the mass became invariable. Then, the peanut vines were thoroughly pulverized by the grinder. The powdery peanut vines of 48 g were added to 0.8 l of deionized water, and the temperature was raised to 370 K for 100 min. The supernate was obtained by centrifugation and stored in the refrigerator for further use.

Synthesis of ICNCs

The ICNCs synthesis was performed by adding 100 ml of peanut vine extracts to 50 ml of 0.24 M $FeCl_3$ and $CuCl_2$ mixed solution over 3 h, under the condition of persistent and mighty stirring. The precipitate was separated by centrifugation at 4200 rpm for 20 min and washed three times with deionized water. Finally, the adsorbent of ICNCs was dried for 12 h at 333 K. Figure 1 illustrates the synthesis mechanism of ICNCs.

Characterization

The specific surface area (S_{BET}) and pore size distribution of ICNCs were measured by the N_2 adsorption-desorption isotherms at 77 K (BET, JW-BK100A, CN). The surface morphology of ICNCs was observed by scanning electron microscope (SEM, FEI Quanta 200 FEG, NED). The surface functional groups of ICNCs were determined using Fourier transform infrared spectrometer (FT-IR, PerkinElmer Spectrum Two, USA). X-ray photoelectron spectroscopy was used to analyze the surface chemical composition of ICNCs (XPS, Thermo ESCALAB 250XI, USA).

Adsorption Experiments

The batch experiments for PFX and ENR adsorption on ICNCs were performed. The working solutions with different concentrations of PFX and ENR were procured by diluting the stock solution with deionized water. The accurate amount of ICNCs and 20 ml PFX or ENR working solution with different concentrations at various pHs (2-10) were added in 50 ml Erlenmeyer flasks. The pH was adjusted by adding 0.1 M HCl or NaOH solution. The mixtures were shaken in a shaking incubator with a speed of 130 rpm. After a requisite duration of time (5-480 min), the solutions were extracted by centrifugation at 10000 rpm for 4 min.

The surplus concentration of PFX was determined by the ultraviolet-visible spectrophotometer (TU-1810, CN) at 275 nm, similarly, the concentration of ENR was determined at 276 nm. The adsorption capacity of PFX or ENR on ICNCs at time t min, q_t (mg/g), and removal rate R (%) were calculated by the following Eqs. (1) and (2):

$$q_t = \frac{(C_0 - C_t)V}{m} \quad (1)$$

$$R(\%) = \frac{100(C_0 - C_t)}{C_0} \quad (2)$$

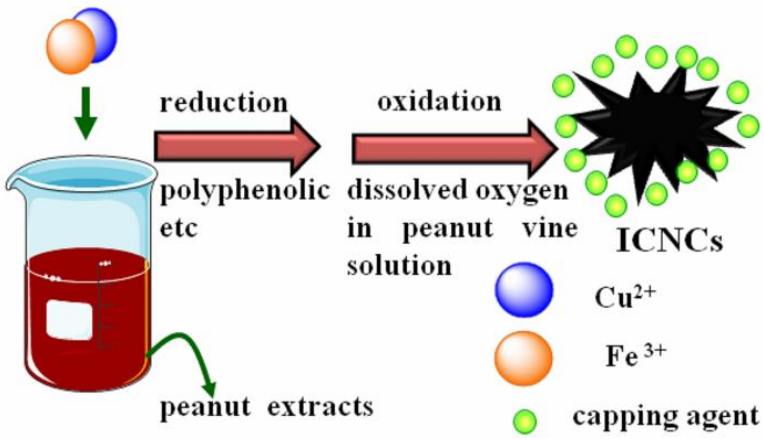

Fig. 1. Synthesis mechanism of ICNCs.

where C_0 and C_t (mg l^{-1}) are the concentrations of PFX or ENR at initial moment and time t (min), respectively. V (l) was the volume of the PFX or ENR solution, and m (g) was the mass of ICNCs.

RESULTS AND DISCUSSION

Characterization of ICNCs

The N_2 adsorption-desorption isotherms of ICNCs at 77 K and pore size distribution were illustrated in Fig. 2. A Type-Ⅳ isotherm with a hysteresis loop was observed. It was attributed to the capillary condensation suggesting the presence of mesoporous matrix in ICNCs [27]. The specific surface area of ICNCs was 27.81 m^2 g^{-1}. The total pore volume was 0.185 cm^3 g^{-1} with an average pore size of 26.608 nm. Micropore volume and mesopore volume were 0.0085 and 0.1765 cm^3 g^{-1}. This proved that ICNCs was mainly mesoporous material.

The SEM image of ICNCs is shown in Fig. 3a, ball-shaped and irregularly shaped nanoparticles of ICNCs with different dimensions were observed [28]. The particles of ICNCs were polydispersed ranging roughly from 100 to 350 nm. As can been seen in Fig. 3a, some ICNCs clusters were possibly caused by the aggregation of ICNCs during sample preparation.

As shown in Fig. 3b, the elemental composition of ICNCs was measured using EDS spectra analysis. ICNCs were sputter-coated with gold to insure a competent conductivity before SEM observation. The quantitative analysis was 61.13% C, 21.08% O, 6.91% N, 10.26% Fe and 0.61% Cu, respectively, indicating that biomolecules such as polyphenolic and flavonoid were grafted on the surface of ICNCs, which played a significant role in preventing aggregation and improving dispersion and stability [25,28].

The surface chemical compositions of ICNCs and their valence states were determined by XPS. Figure 4a revealed the presence of C, O, N, Fe and Cu in ICNCs. The high-resolution spectrum of C1s is shown in Fig. 4b, three types of C are present on the surface of ICNCs such as C-C (284.76 eV), C-O (286.47 eV) and C=O (288.67 eV), respectively [29]. Figure 4c suggested that the peak at 531.77 eV is ascribed to the existence of Fe-O/Cu-O, while the peak at 532.97 eV is the signal of C=O, C-OH or C-O-C functional groups [28,30]. The C, N and O may come from biomolecules in peanut vine extracts, indicating that polyphenolic and flavonoid from peanut vine extracts formed capping agents of ICNCs. Figure 4d illustrates the signals of Fe 2p and Cu 2p. The locations of Fe 2p1/2 and 2p3/2 core levels were 711.57 and 725.07 eV, respectively, confirmed the existence of iron oxide [28]. The peaks at 953.07 and 933.37 eV were attributed to Cu^{2+} in CuO [31]. In general, the surfaces of ICNCs were composed of polyphenolic and other C, O-containing functional groups.

The functional groups of PFX, ENR, ICNCs before and after adsorption of PFX and ENR were characterized using

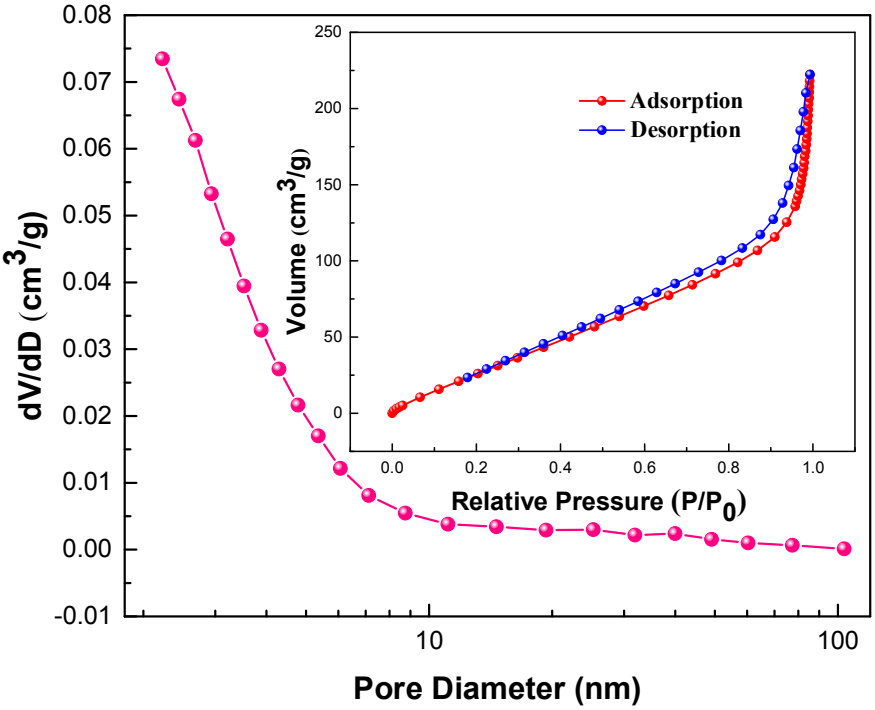

Fig. 2. N_2 adsorption isotherm and pore size distribution for ICNCs.

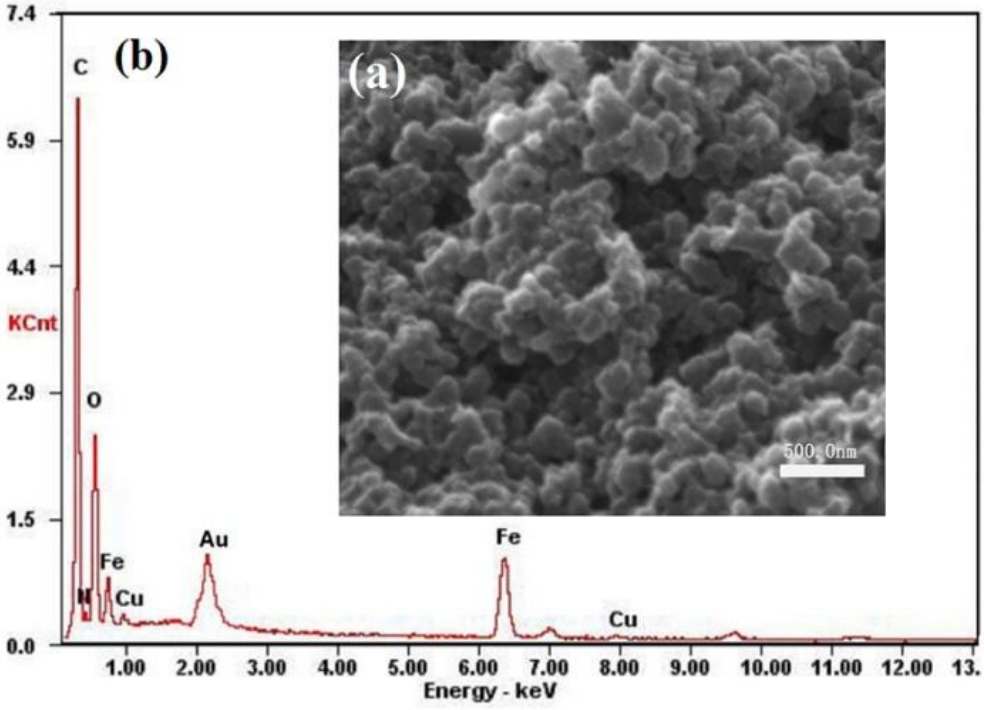

Fig. 3. (a) SEM micrographs and (b) EDS spectra of ICNCs.

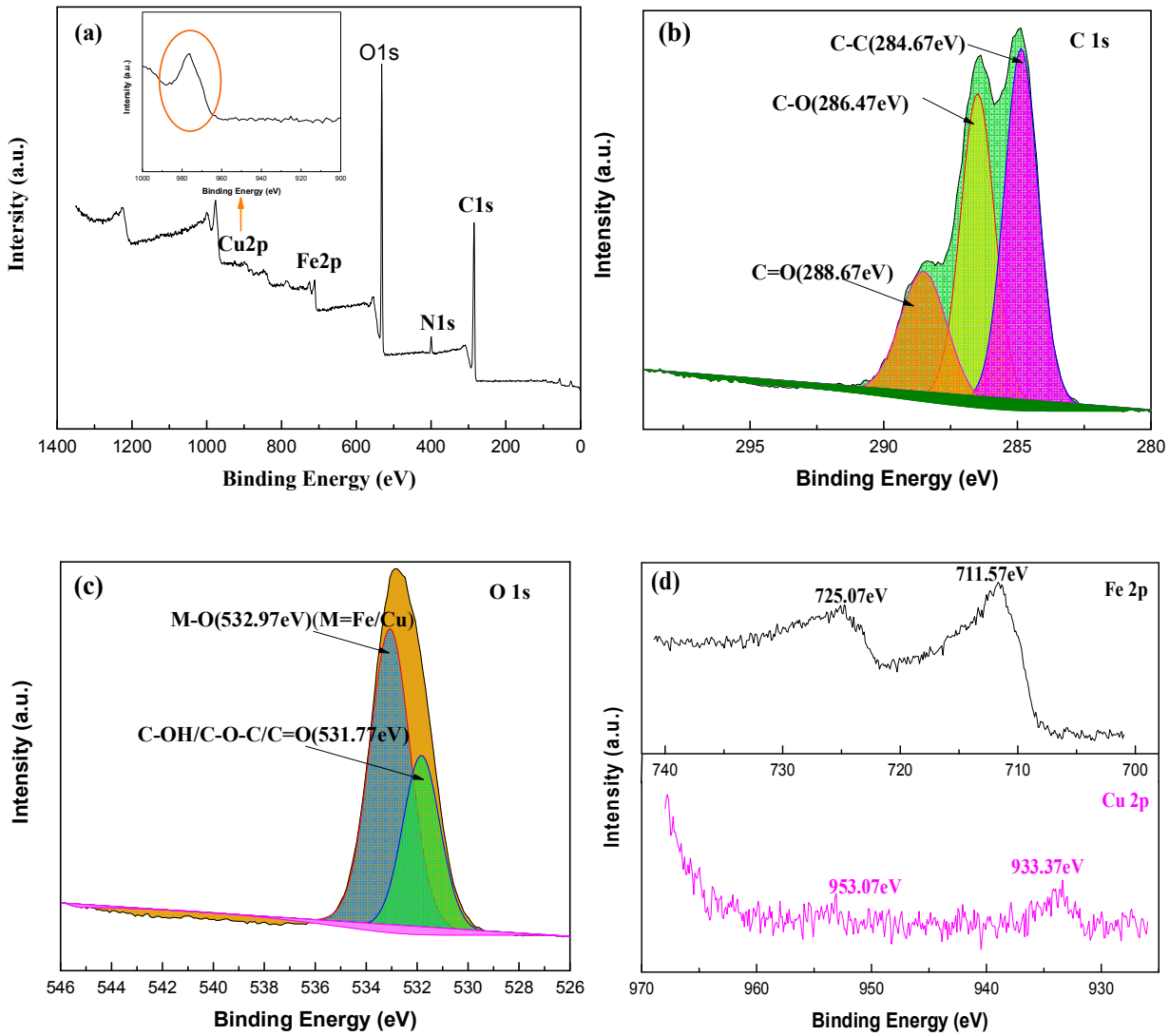

Fig. 4. (a) XPS survey spectrum, (b) C 1s spectrum of ICNCs, (c) O 1s spectrum of ICNCs and (d) Fe 2p and Cu 2p spectrum of ICNCs.

KBr pellet method by FT-IR analysis and the result is shown in Fig. 5. As for ICNCs, the band at 3415.07 cm^{-1} was due to the stretch vibration of O-H or adsorbed water [32]. The characteristic peak at 2925.54 cm^{-1} represented the C-H stretch of aliphatics. The peak caused by the vibrations of C=O was found at 1728.91 cm^{-1}. A peak at 1629.53 cm^{-1} was associated with the C=C stretching of aromatic rings in ICNCs, which was related to the polyphenols or flavonoid in peanut vine extracts [33], so, the band at 1070.66 cm^{-1} was mainly produced by C-O-C stretching vibration. The peak appeared at 586.09 cm^{-1} refer to Fe-O/Cu-O stretching in metal oxides [34]. FTIR analysis proved that the molecular structure of ICNCs mainly contains C=C, C-H, C=O, -OH and Fe/Cu-O functional groups.

For PFX, a peak was observed at 1715.34 cm^{-1} because of the C=O group of carboxyl. Peak at 1629.53 cm^{-1} implied the vibrations of C=C of aromatic rings in PFX. Similarly, ENR had the same functional groups as shown in Fig. 5b.

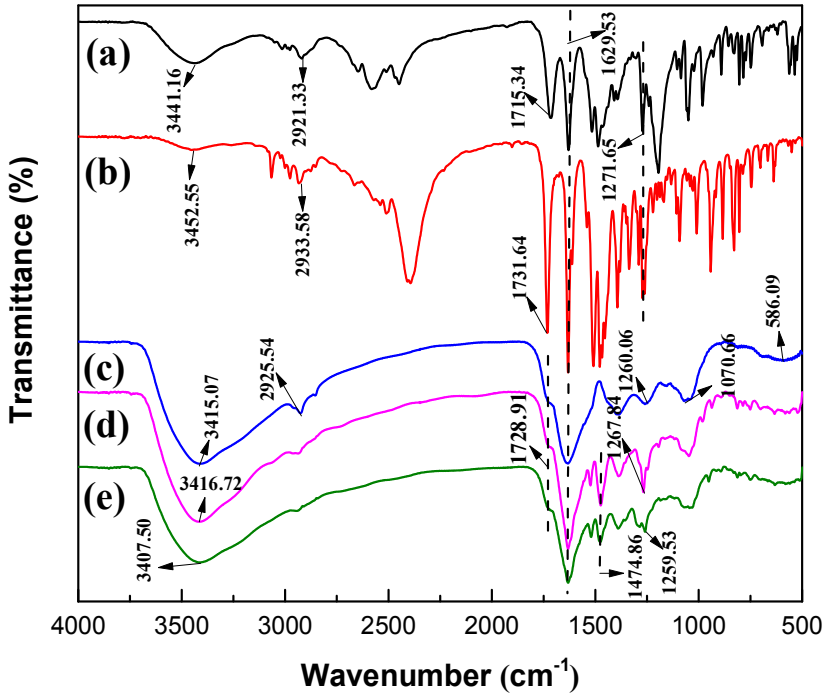

Fig. 5. FT-IR spectra of (a) PFX, (b) ENR, (c) ICNCs, (d) ICNCs-PFX and (e) ICNCs-ENR.

The spectral profile of the ICNCs with adsorbed PFX or ENR showed differences from the ICNCs due to the adsorbed PFX or ENR. In comparison with the FTIR spectra of ICNCs, the change in intensity of peak 1260.06 cm^{-1} and the new peaks at 1474.86 cm^{-1} belonging to the C-C stretching (in-ring) of aromatic rings proved the presence of PFX or ENR on ICNCs indicating that PFX or ENR was successfully adsorbed on ICNCs.

Adsorption Kinetic Studies

The experimental data for PFX and ENR adsorbed on the ICNCs were analyzed by pseudo-first-order, pseudo-second-order and intra-particle diffusion models. The kinetic equations and χ^2 were expressed as Eqs. ((3)-(6)). Nonlinear χ^2 was often used to inspect the degree of deviation between model data and experimental data. The value of χ^2 was smaller, indicating a smaller degree of deviation.

Pseudo-first-order:

$$q_t = q_e\left(1-\exp^{-k_1 t}\right) \quad (3)$$

Pseudo-second-order:

$$q_t = \frac{k_2 q_e^2 t}{1+k_2 q_e t} \quad (4)$$

Intra-particle diffusion:

$$q_t = k_{ti} t^{1/2} + C_i \quad (5)$$

$$\chi^2 = \Sigma \frac{\left(q_{e,exp} - q_{e,cal}\right)^2}{q_{e,exp}} \quad (6)$$

Where q_t and q_e (mg g^{-1}) are the amounts of PFX or ENR adsorbed at time t and equilibrium, respectively. k_1 (1 min^{-1}) and k_2 (g (mg^{-1} min^{-1})) are the pseudo-first-order and pseudo-second-order adsorption rate constants. k_{ti} (mg (g^{-1} $min^{-1/2}$) is the diffusion constant in particles. C_i is a constant related to the boundary layer thickness. $q_{e,exp}$ and $q_{e,cal}$ are experimental and calculated adsorption capacity of ICNCs.

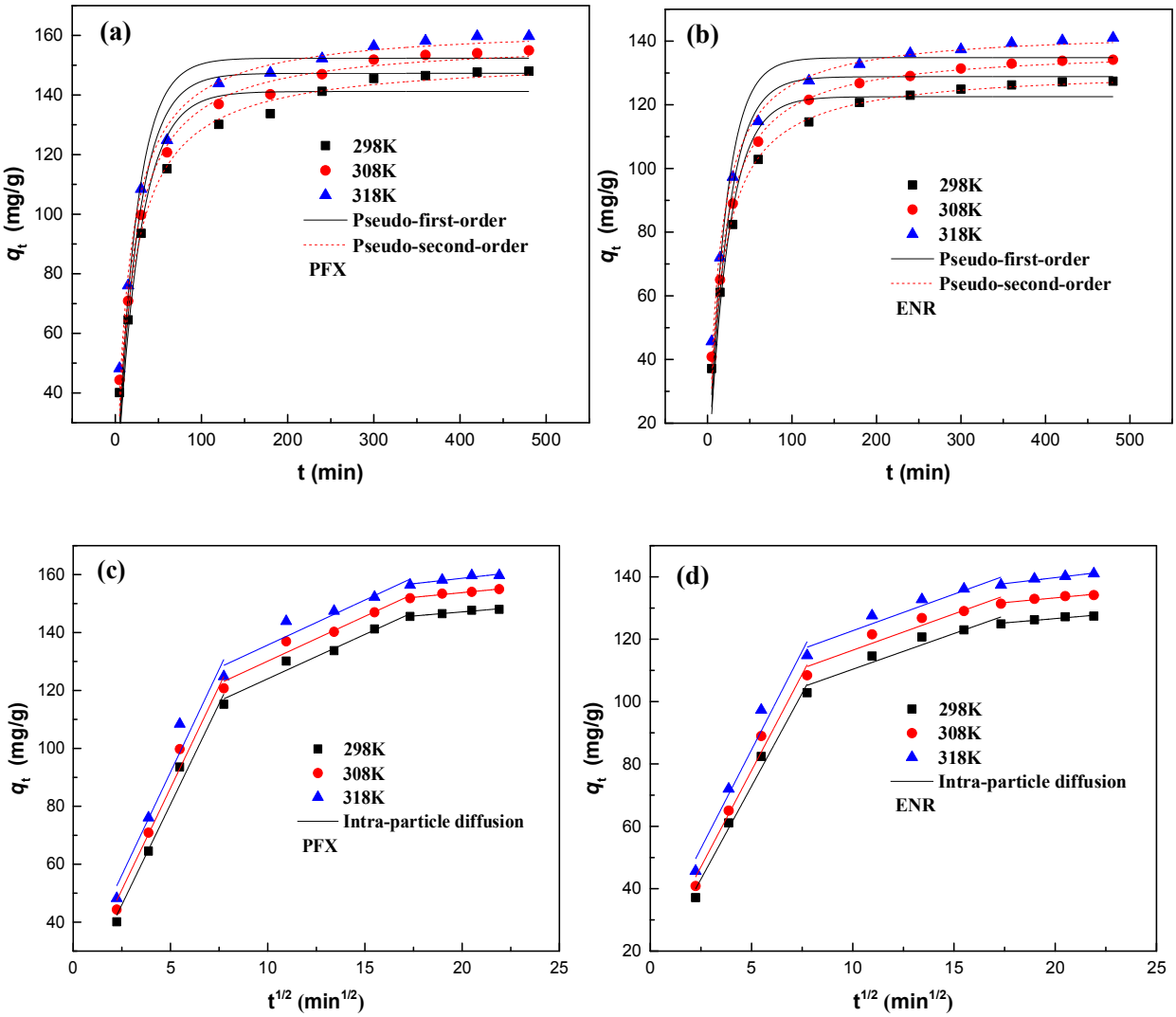

Fig. 6. Nonlinear fitting of (a) PFX and (b) ENR experimental data with pseudo-first-order, pseudo-second-order and intra-particle diffusion of (c) PFX and (d) ENR (C_0 = 100 mg g^{-1}, contact time = 360 min, adsorbent dosage = 0.5 g l^{-1}, pH = 5.17 for PFX; pH = 4.99 for ENR).

The regression analysis of experimental data, kinetic parameters and χ^2 of models were illustrated in Fig. 6 and Table 1. The uptake amount of PFX and ENR increased promptly, and then slowly until the adsorption balance was reached. The equilibrium adsorption amounts q_{e2} calculated by the pseudo-second-order model were approximate to the experimental adsorption capacity q_{exp}. As indicated by $R^2 > 0.98$ and $\chi^2 < 2.3$, the pseudo-second-order model fitted better with the data of PFX or ENR on ICNCs than the pseudo-first-order model, which was accorded with the results from Fig. 6. The pseudo-second-order rate constant k_2 showed a gradual augment with increasing temperature, indicating that the adsorption process was more active at high temperature.

In order to illustrate the diffusion process of PFX and ENR, the intra-particle diffusion model was used to describe

Table 1. Parameters of Adsorption Kinetic for PFX and ENR onto ICNCs

Model	PFX			ENR		
	298 K	308 K	318 K	298 K	308 K	318 K
Pseudo-first-order kinetic model						
k_1 (1 min^{-1})	0.0374	0.0399	0.0435	0.0413	0.0433	0.0482
q_{e1} (mg g^{-1})	141.18	147.29	152.37	122.54	128.83	134.80
R^2	0.9458	0.9368	0.9331	0.9473	0.9427	0.9323
χ^2	9.7290	10.8765	10.9353	7.9192	8.5671	9.0539
pseudo-second-order kinetic model						
k_2*10^4 (g mg^{-1} min^{-1})	3.4980	3.6576	3.9329	4.6714	4.7063	5.1024
q_{e2} (mg g^{-1})	152.48	158.45	163.17	131.32	137.74	143.51
q_{exp} (mg g^{-1})	148.02	154.97	159.72	127.39	134.14	141.01
R^2	0.9913	0.9899	0.9896	0.9938	0.9927	0.9919
χ^2	2.0092	2.1536	2.0616	1.2435	1.4479	1.3739
Intra-particle diffusion model						
k_{t1} (mg g^{-1} $min^{-1/2}$)	13.8725	14.0515	14.2007	11.9184	12.3498	12.6413
C_1	11.30	16.02	20.75	13.27	16.13	21.33
R	0.9737	0.9676	0.9349	0.9792	0.9721	0.9540
k_{t2} (mg g^{-1} $min^{-1/2}$)	3.0679	3.0966	3.1085	2.2898	2.3292	2.3442
C_2	93.34	99.15	104.59	87.48	93.19	99.28
R	0.9631	0.9488	0.8935	0.9116	0.8954	0.9034
k_{t3} (mg g^{-1} $min^{-1/2}$)	0.5637	0.6523	0.7568	0.5538	0.6035	0.7692
C_3	135.85	140.74	143.61	115.54	121.19	124.36
R	0.8551	0.9538	0.8614	0.9016	0.9040	0.9369

the adsorption data [35]. Figures 6c and d illustrate that the adsorption process of PFX and ENR onto ICNCs involved three stages. Firstly, PFX or ENR molecules were transferred from solution to the external surface of ICNCs. Secondly, the uptake of PFX and ENR was increased gradually, which was pore-diffusion or intra-particle diffusion stage. Finally, the adsorption equilibrium of PFX and ENR adsorbed on the ICNCs was achieved. In addition, k_{ti} showed a decreasing trend of $k_{t1} > k_{t2} > k_{t3}$ during the whole adsorption process of ICNCs. Meanwhile, none of fitting straight lines pass origins, reflecting that the intra-particle diffusion was not the only rate-determining step for PFX and ENR adsorbed on

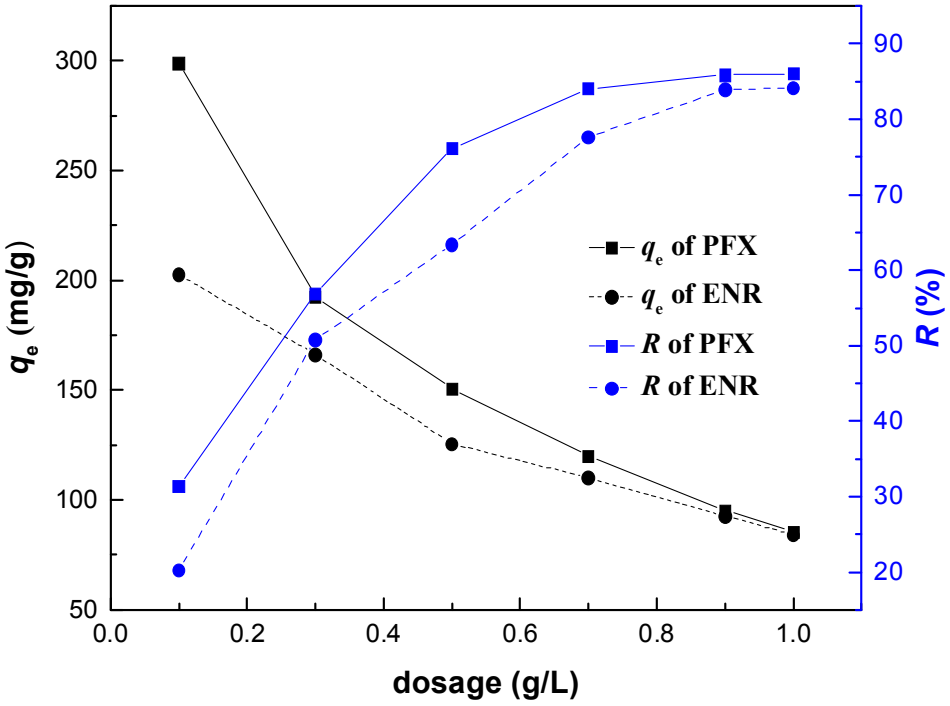

Fig. 7. Effect of adsorbent dosage on the adsorption capacity of ICNCs (C_0 = 100 mg l^{-1}; contact time = 360 min; T = 298 K, pH = 5.17 for PFX; pH = 4.99 for ENR).

ICNCs, membrane diffusion process also played a role in the adsorption process [36]. Hence, the 360 min was selected as an appropriate contact time for the subsequent experiments.

Effect of Adsorbent Dosage on PFX and ENR Adsorption

The trends of equilibrium adsorption amount and removal rate of PFX and ENR caused by the increase of ICNCs dosage are shown in Fig. 7. The PFX removal efficiency of ICNCs increased from 31.39 to 86.01% while the adsorption capacity of ICNCs decreased from 298.95 to 85.58 mg g^{-1} with increasing the adsorbent dosage from 0.1 to 1 g l^{-1}. The increase of removal rate was attributed to more availability of active sites with rising the adsorbent dosage. Due to fierce competition of adsorbent, the adsorption capacity of unit mass was decreased accordingly. Similarly, the ENR removal efficiency of ICNCs increased from 20.26 to 84.14% and the ENR adsorption capacity of ICNCs decreased from 202.60 to 84.15 mg g^{-1} with increasing the dosage of ICNCs from 0.1 to 1 g l^{-1}. The ICNCs dosage of 0.5 g l^{-1} was selected because of its good removal efficiency and adsorption capacity to PFX and ENR at the same time.

Adsorption Mechanism

The point of zero charge (pH_{PZC}) is defined as the pH value of zero net charge on the surface of ICNCs. The pH_{PZC} of ICNCs was determined by the following method [37]: 20 mg of ICNCs was mixed with 20 ml of 0.01 M sodium chloride solution and the pH was adjusted with 0.1 M NaOH or HCl solution. The pH of the supernatant was recorded after 6 h of oscillation. The pH of the initial solution and final solution designated as $pH_{initial}$ and pH_{final}, respectively. ΔpH was defined as the difference value between the pH of initial solution ($pH_{initial}$) and that of the ultimate solution (pH_{final}). The pH_{pzc} of ICNCs was the value that the curve ΔpH vs. $pH_{initial}$ crosses the abscissa. The pH_{pzc} of ICNCs was 3.56. The surface net charge of ICNCs was positive at

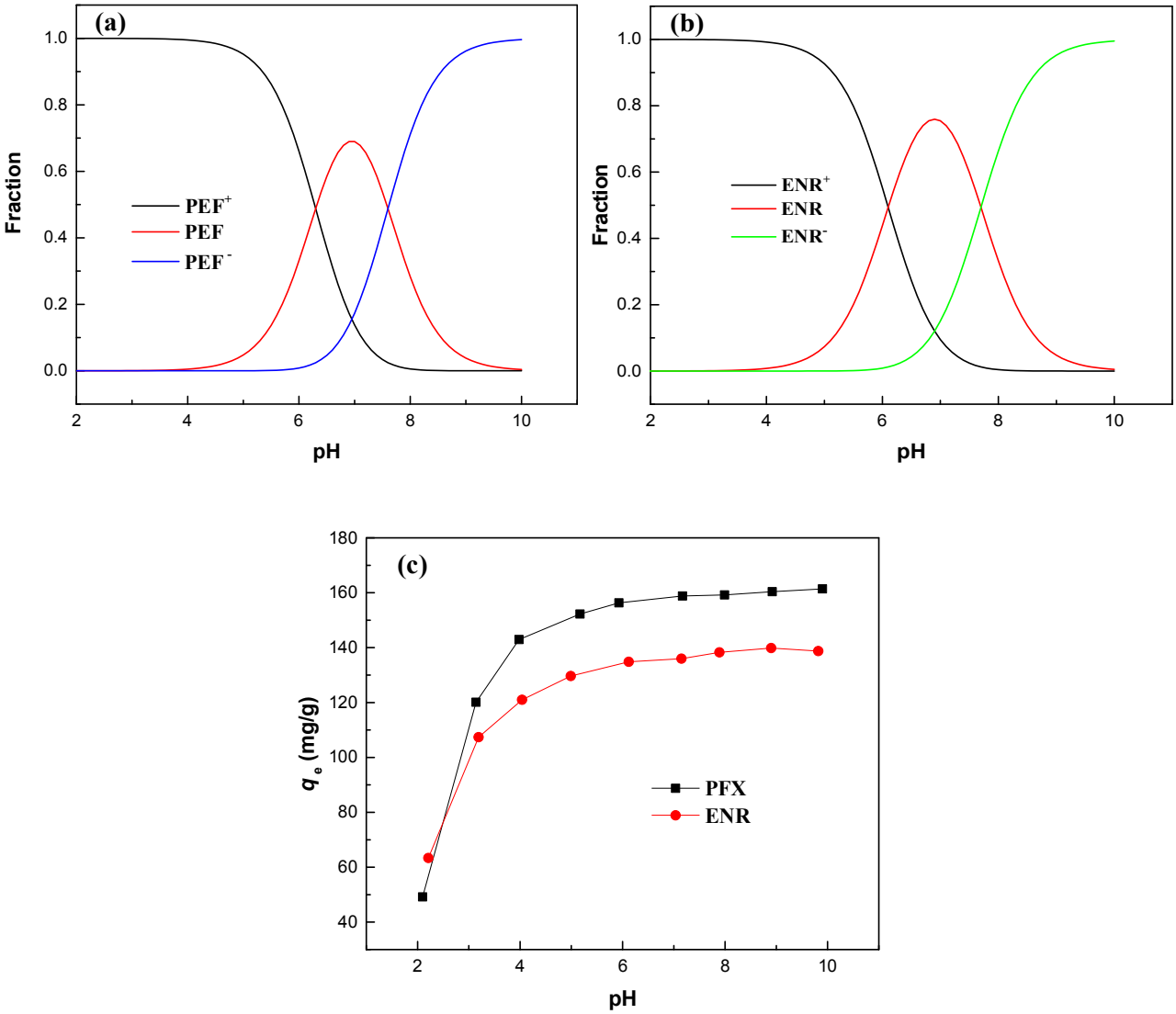

Fig. 8. The distribution coefficient of (a) PFX and (b) ENR, (c) adsorption capacity of PFX or ENR at different pHs (C_0 = 100 mg l^{-1}, adsorbent dosage = 0.5 g l^{-1}, contact time = 360 min).

the range of pH < pH_{pzc} and negative at the range of pH > pH_{pzc}.

The values of pH were another considerable factor affecting the adsorption capacity of ICNCs. Because of the presence of the carboxyl and amino groups, both PFX (pK_{a1} = 6.3, pK_{a2} = 7.6) and ENR (pK_{a1} = 6.1, pK_{a2} = 7.7) have two pK_as. As shown in Figs. 8a and b, with the pH increasing, PFX and ENR existed in three forms in the solution: At pH < pK_{a1}, the amidogen was protonated and the PFX^+ or ENR^+ was the main ionic form. At pK_{a1} < pH < pK_{a2}, zwitterionic form PFX^0 or ENR^0 became the primary form due to the charge balance of carboxyl and amidogen. At pH > pK_{a2}, the anion of PFX^- or ENR^- was prevalent because of the deprotonation of the carboxyl group [38].

The effect of the initial solution pH on the adsorption of PFX and ENR by the ICNCs is shown in Fig. 8c. The

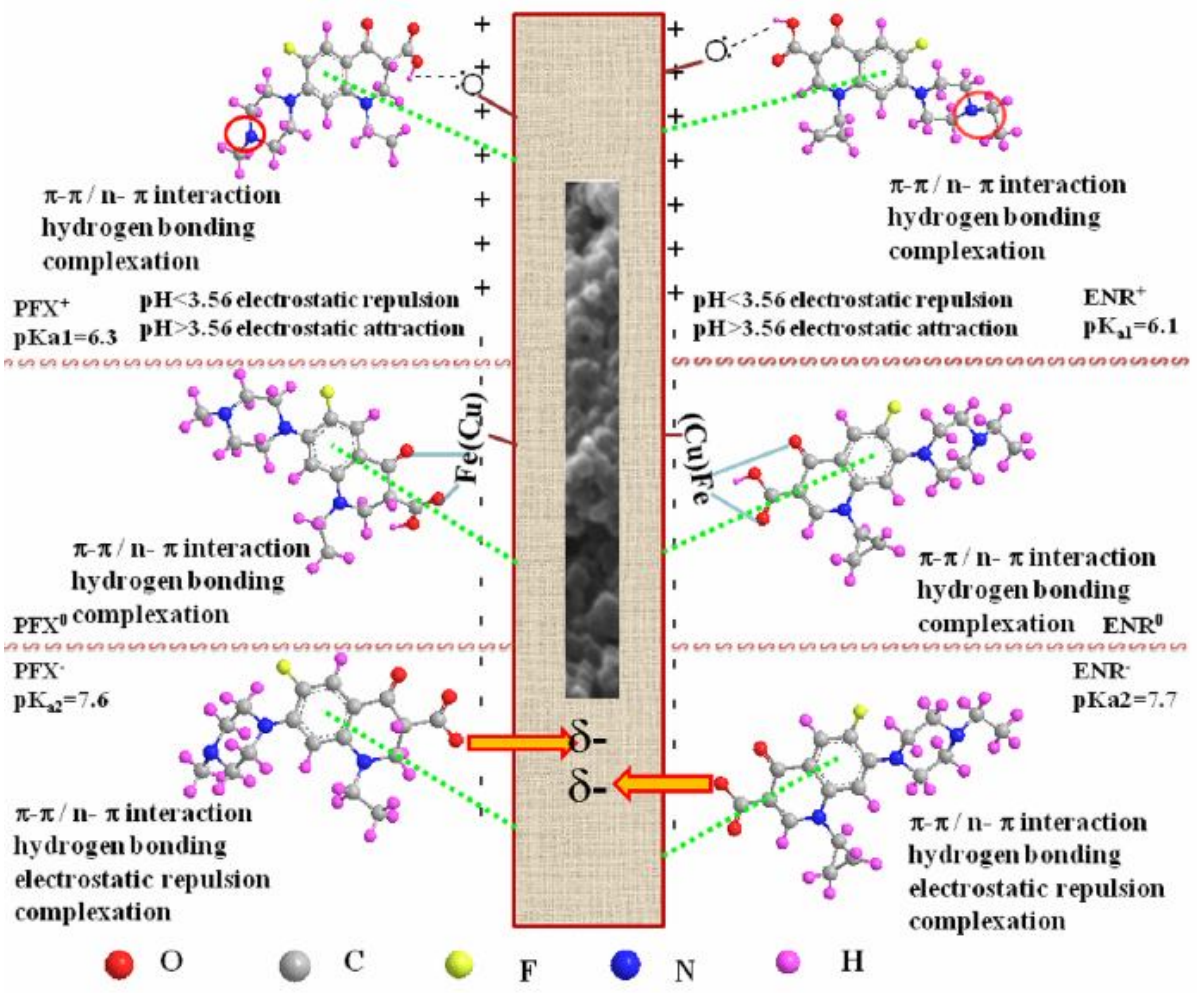

Fig. 9. Schematic diagram of adsorption mechanism of PFX and ENR on ICNCs.

schematic diagram of the adsorption mechanisms of PFX and ENR on ICNCs are shown in Fig. 9. The uptake of PFX on ICNCs increased from 49.18 to 161.42 mg g^{-1} when pH increased from 2 to 10. Hydrogen bonding formed between carbonyl or hydroxy group in PFX and hydroxy or carbonyl on the surface of ICNCs. The π-π interaction mainly happened between the ICNCs and PFX or ENR [39]. Hydrogen bonding, π-π interaction and complexation existed continuously in the adsorption process. At pH < 3.56, ICNCs exhibited a low adsorption capacity for PFX. It was possibly due to the electrostatic repulsive interaction between protonated antibiotics (PFX^+) and the positively charged surface of ICNCs. At 3.56 < pH < 6.3, an ascent value of q_e for PFX was observed, because of the electrostatic attraction between the protonated antibiotics (PFX^+) and negatively charged surface of ICNCs. At 6.3 < pH < 7.6, PFX in zwitterionic form was more hydrophobic than its cation or anion form, so the value of q_e was slightly changed [40]. At pH > 7.6, a steady value of q_e was seen with increase the pH value. The PFX^- and the negative charge on the ICNCs surface repelled each other. The lone pair electrons of O (*e.g.* -OH) in PFX or ENR as n-electron donors directly interacted with the π-electron deficient sites of ICNCs as π-acceptors. Furthermore, the n-π interaction enhanced by ionized -OH in PFX at high pH, so it offset the electrostatic repulsion. The adsorption capacity of

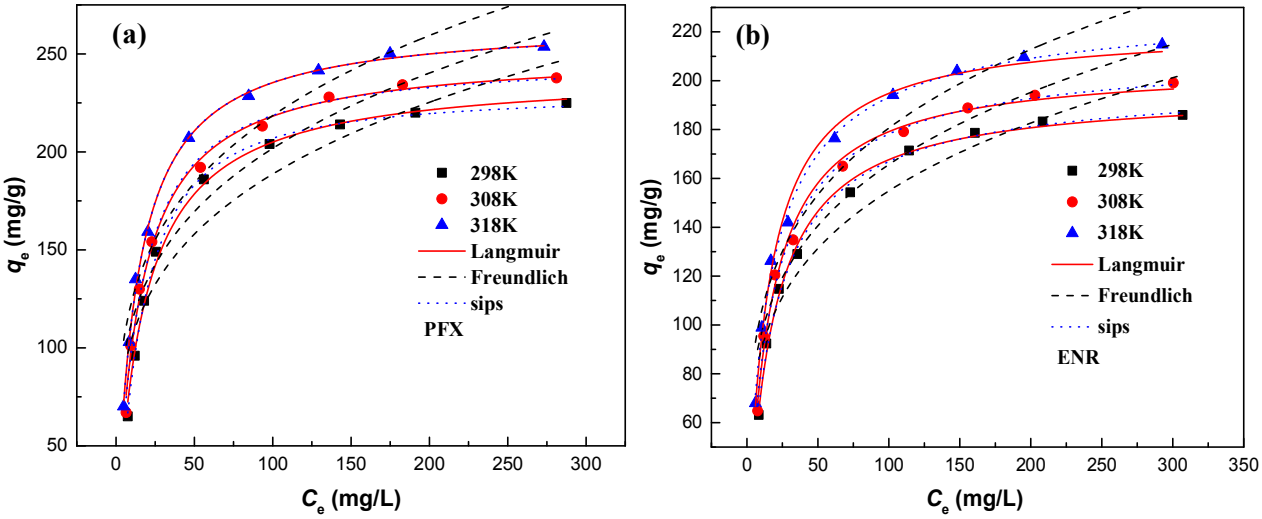

Fig. 10. Adsorption isotherms of (a) PFX and (b) ENR on ICNCs at different temperatures (contact time = 360 min, adsorbent dosage = 0.5 g l^{-1}, unadjusted pH).

ICNCs for ENR, increased from 63.37 to 143.74 mg g^{-1}, showed a similar trend with the increase of pH.

Adsorption Isotherm Studies

Langmuir, Freundlich and Sips isotherm models were used to explore the adsorption behavior. The isotherm equations were given as Eqs. (7)-(9),

Langmuir isotherm model:

$$q_e = \frac{K_L q_m C_e}{1 + K_L C_e} \tag{7}$$

Freundlich isotherm model:

$$q_e = K_F C_e^{1/n} \tag{8}$$

Sips isotherm model:

$$q_e = \frac{q_{ms}(K_s C_e)^m}{1 + (K_s C_e)^m} \tag{9}$$

where K_L (l mg^{-1}) and q_m (mg g^{-1}) are the Langmuir adsorption equilibrium constant and the maximum monolayer adsorption capacity, respectively. n is the tendency of adsorption and K_F ((mg g^{-1}) (l $mg^{-1})^{1/n}$) is the Freundlich constant. K_s and q_{ms} are the constant and maximum adsorption capacity of the Sips isotherm model, respectively. m represents the model index, which is equivalent to Langmuir when m = 1.

The adsorption isotherms and model parameters of PFX and ENR on ICNCs at 298, 308 and 318 K are illustrated in Fig. 10 and Table 2. The uptake amount of equilibrium adsorption increased with increasing concentrations of PFX and ENR. Equation parameters, correlation coefficients (R^2) and χ^2 were applied to estimate the capability of the isotherm models about nonlinear data fitting. The Langmuir isotherm model assumed a uniform distribution of the adsorption sites, the adsorption process was monolayer adsorption and dynamically balanced [41]. Both q_m and K_L were increased with increasing temperature, and the maximum monolayer adsorption amount of PFX and ENR were 240.70 and 1 95.97 mg g^{-1} at 298 K, respectively. The experimental data were well described by the Langmuir model with $R^2 > 0.99$ and $\chi^2 < 1.7$.

Freundlich model was used to describe the multilayer adsorption of heterogeneous surfaces [42]. The values of R^2 (< 0.93) and χ^2 (>12) indicated that the Freundlich model was unadvisable to describe the equilibrium adsorption data.

Table 2. Adsorption Isotherm Parameters for PFX and ENR on ICNCs at Different Temperatures

Model	PEF			ENR		
	298 K	308 K	318 K	298 K	308 K	318 K
Langmuir						
q_m (mg g^{-1})	240.70	250.97	266.52	195.97	206.66	222.03
K_L (l mg^{-1})	0.057	0.067	0.075	0.059	0.065	0.071
R^2	0.9955	0.9943	0.9984	0.9947	0.9926	0.9930
χ^2	1.2095	1.6917	0.3962	0.6124	1.0423	0.9615
Freundlich						
K_F (mg g^{-1} (l mg^{-1})$^{1/n}$)	58.06	63.38	70.04	51.74	55.69	60.76
1/n	0.26	0.25	0.25	0.2381	0.2367	0.2366
R^2	0.8823	0.8984	0.8975	0.9136	0.9163	0.9225
χ^2	26.3916	26.2408	27.6656	12.2965	13.9802	14.2810
Sips						
q_{ms} (mg g^{-1})	230.56	248.24	266.26	200.17	212.47	232.89
Ks (l mg^{-1})	0.063	0.068	0.076	0.057	0.061	0.064
m	1.18	1.04	1	0.93	0.91	0.85
R^2	0.9988	0.9936	0.9981	0.9946	0.9926	0.9955
χ^2	0.1715	1.4792	0.3902	0.6276	1.1024	0.6617

Table 3. Comparison of Adsorption Capacity of PFX and ENR on Different Adsorbents

Adsorbent	Adsorbate	q_{max} (mg g^{-1})	Ref.
Iindustrial paper sludge	ENR	44.44	[15]
Natural zeolite	ENR	19.34	[16]
Clay minerals	ENR	7.19	[43]
Ligno-cellulosic substrate	ENR	91.50	[44]
Polyacrylic acid-grafted-carboxylic	ENR	13.40	[17]
Na-montmorillonite	ENR	160.50	[43]
ICNCs	ENR	222.03	This work
Halloysite nanotubes	PFX	40.49	[14]
Oxidized multiwalled carbon nanotube	PFX	212.46	[7]
ICNCs	PFX	266.52	This work

Sips isotherm has three parameters, which is regarded as a combination of Langmuir and Freundlich models [45,46]. Sips parameter, q_{ms}, was equal to the q_m of Langmuir parameter in high adsorbate concentrations [36]. Sips model showed a similar fitting for the experimental data in Figs. 10a and b, which was close to the trend of the Langmuir model. The predicted maximum adsorption q_{ms} and q_m were also approximate. The higher R^2 and lower χ^2 value suggested that the Sips isotherm model was suitable to describe the uptake of PFX or ENR onto the ICNCs, and the adsorption process included homogeneous and nonhomogeneous adsorptions [47,48]. Therefore, the adsorption behavior of PFX and ENR on ICNCs was well described by Langmuir and Sips models.

The comparisons of PFX and ENR adsorption capacity onto different adsorbents are shown in Table 3. In this study, the uptake amount of PFX and ENR on ICNCs reached 240.70 and 195.97 mg g^{-1} at 298 K, which was significantly high adsorption capacity compared with other absorbents. Overall, ICNCs could be a promising material for the treatment of antibiotic wastewater.

Thermodynamic Parameters

Three thermodynamic parameters: Gibbs free energy change ΔG (kJ mol^{-1}), enthalpy change ΔH (kJ mol^{-1}), and entropy change ΔS (kJ mol^{-1} K^{-1}) were computed by the following equations:

$$Kc = \frac{C_{ad}}{C_e} \tag{10}$$

$$\Delta G = -RTlnK_C \tag{11}$$

$$\ln K_C = \frac{\Delta S}{R} - \frac{\Delta H}{RT} \tag{12}$$

where C_e and C_{ad} (mg g^{-1}) are the concentrations of adsorbate in solution and adsorbent at adsorption balance, respectively. K_C represents the equilibrium constant of thermodynamics. R (8.314 J mol^{-1} K^{-1}) is the universal gas constant, and T (K) represents the Kelvin temperature.

The computation results of thermodynamic parameters are summarized in Table 4. A negative ΔG value indicated that the adsorption progress for PFX and ENR was spontaneous [49]. Moreover, the absolute value of ΔG enhanced with increasing temperature demonstrating the endothermic nature of PFX and ENR adsorbed by ICNCs, which was consistent with negative values of ΔH [42]. The positive values of ΔS suggested the randomness and irregularity of PFX and ENR on the sample-solution interface [42].

Recycling of ICNCs

Desorption of PFX and ENR from ICNCs was conducted by using 0.1 M HCl solution. The recyclability of ICNCs was illustrated in Fig. 11. The adsorption ability of the recycled ICNCs for PFX and ENR remained at 128.56 and 103.56 mg g^{-1}, respectively, over three adsorption-desorption cycles, indicating that hydrochloric acid can be taken as a good recycling agent. So, it was stated that ICNCs can be renewed easily with HCl solution.

CONCLUSIONS

In this study, the ICNCs prepared by peanut vine extracts were applied as adsorbents to remove PFX or ENR from aqueous solutions. Experimental results revealed that the maximum monolayer adsorption capacity of ICNCs for PFX and ENR reached up to 240.70 and 195.97 mg g^{-1} at 298 K, respectively. Electrostatic, π-π and n-π interactions, hydrogen bonding and complexation were the primary driving forces for the removal of PFX and ENR by ICNCs. Besides, the PFX and ENR adsorption data fitted well with the Langmuir and Sips models, and the adsorption of PFX and ENR was a spontaneous and endothermic process. Additionally, it was found that the adsorption kinetic data successfully followed the pseudo-second-order model. Furthermore, the ICNCs showed good regeneration capability, which was an important property for practical applications. Based on the results presented, the ICNCs could be a promising material to remove antibiotic PFX or ENR.

ACKNOWLEDGEMENTS

This project is funded by Science and Technology Department of Henan Province (162102210002), the Processing and Efficient Utilization of Biomass Resources of

Table 4. Thermodynamic Parameters for PFX and ENR on ICNCs at Different Temperatures

Temperature (K)	PFX			ENR		
	ΔG (kJ mol^{-1})	ΔH (kJ mol^{-1})	ΔS (J mol^{-1} K^{-1})	ΔG (kJ mol^{-1})	ΔH (kJ mol^{-1})	ΔS (J mol^{-1} K^{-1})
298	-6.95			-7.37		
308	-7.90	19.93	90.27	-8.04	13.85	71.16
318	-8.75			-8.79		

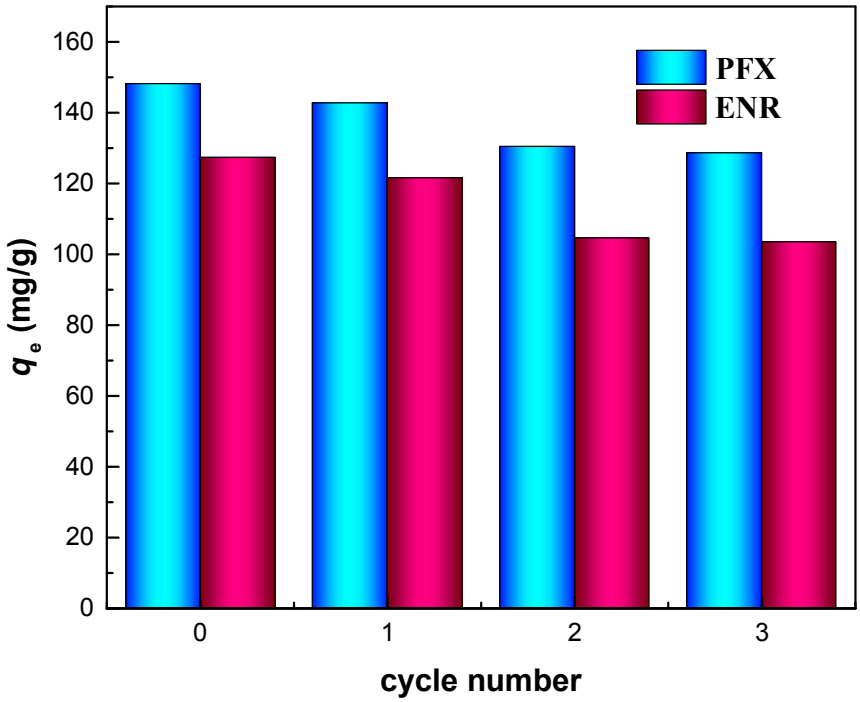

Fig. 11. Effect of cycle number on the adsorption capacity of ICNCs (C_0 = 100 mg l^{-1}; contact time = 360 min; T = 298 K, pH = 5.17 for PFX; pH = 4.99 for ENR).

Henan Center for Outstanding Overseas Scientists (GZS2018004).

REFERENCES

[1] Xiang, Y.; Yang, X.; Xu, Z.; Hu, W.; Zhou, Y.; Wan, Z.; Yang, Y.; Wei, Y.; Yang, J.; Tsang, D. C. W., Fabrication of sustainable manganese ferrite modified biochar from vinasse for enhanced adsorption of fluoroquinolone antibiotics: Effects and mechanisms. *Sci. Total Environ.* **2020**, *709*, 136079, DOI: 10.1016/j.scitotenv.2019.136079.

[2] Dantas, G.; Sommer, Morten O. A.; Oluwasegun, R. D.; Church, G. M., Bacteria subsisting on antibiotics. *Science* **2008**, *320*, 100-103, DOI: 10.1126/science.1155157.

[3] Khanday, W. A.; Ahmed, M. J.; Okoye, P. U.; Hummadi, E. H.; Hameed, B. H., Single-step pyrolysis of phosphoric acid-activated chitin for efficient adsorption of cephalexin antibiotic. *Bioresour. Technol.* **2019**, *280*, 255-259, DOI: 10.1016/j.biortech.2019.02.003.

[4] Fu, H.; Li, X.; Wang, J.; Lin, P.; Chen, C.; Zhang, X.; Suffet, I. H., Activated carbon adsorption of quinolone antibiotics in water: Performance, mechanism, and modeling. *J. Environ. Sci.* **2017**, *56*, 145-152, DOI: 10.1016/j.jes.2016.09.010.

[5] Chen, J.; Liu, Y.; Zhang, J.; Yang, Y.; Hu, L.; Yang, Y.; Zhao, J.; Chen, F.; Ying, G., Removal of antibiotics from piggery wastewater by biological aerated filter system: Treatment efficiency and biodegradation kinetics. *Bioresour. Technol.* **2017**, *238*, 70-77, DOI: 10.1016/j.biortech.2017.04.023.

[6] Beltran, F. J.; Aguinaco, A.; Garcia-Araya, J. F.; Oropesa, A. L., Oropesa, Ozone and photocatalytic processes to remove the antibiotic sulfamethoxazole from water. *Water Res.* **2008**, *42*, 3799-3808, DOI: 10.1016/j.watres.2008.07.019.

[7] Zhou, Y.; He, Y.; Xiang, Y.; Meng, S.; Liu, X.; Yu, J.; Yang, J.; Zhang, J.; Qin, P.; Luo, L., Single and simultaneous adsorption of pefloxacin and Cu(II) ions from aqueous solutions by oxidized multiwalled carbon nanotube. *Sci. Total Environ.* **2019**, *646*, 29-36, DOI: 10.1016/j.scitotenv.2018.07.267.

[8] Liu, X.; Yang, D.; Zhou, Y.; Zhang, J.; Luo, L.; Meng, S.; Chen, S.; Tan, M.; Li, Z.; Tang, L., Electrocatalytic properties of N-doped graphite felt in electro-Fenton process and degradation mechanism of levofloxacin. *Chemosphere* **2017**, *182*, 306-315, DOI: 10.1016/j.chemosphere.2017.05.035.

[9] Choi, K. J.; Son, H. J.; Kim, S. H., Ionic treatment for removal of sulfonamide and tetracycline classes of antibiotic. *Sci. Total Environ.* **2007**, *387*, 247-256, DOI: 10.1016/j.scitotenv.2007.07.024.

[10] Qiu, W.; Zheng, M.; Sun, J.; Tian, Y. ; Fang, M.; Zheng, Y.; Zhang, T.; Zheng, C., Photolysis of enrofloxacin, pefloxacin and sulfaquinoxaline in aqueous solution by UV/H_2O_2, UV/Fe(II), and UV/H_2O_2/Fe(II) and the toxicity of the final reaction solutions on zebrafish embryos, *Sci. Total Environ.* **2019**, *651*, 1457-1468, DOI: 10.1016/j.scitotenv.2018.09.315.

[11] Ma, H.; Yu, B.; Wang, Q.; Owens, G.; Chen, Z., Enhanced removal of pefloxacin from aqueous solution by adsorption and Fenton-like oxidation using NH_2-MIL-88B, *J. Colloid Interface Sci.* **2021**, *583*, 279-287, DOI: 10.1016/j.jcis.2020.09.034.

[12] Mehrjouei, M.; Müller, S.; Möller, D., Energy consumption of three different advanced oxidation methods for water treatment: A cost-effectiveness study, *J. Clean Prod.* **2014**, *65*, 178-183, DOI: 10.1016/j.jclepro.2013.07.036.

[13] Le-Minh, N.; Khan, S. J.; Drewes, J. E.; Stuetz, R. M., Fate of antibiotics during municipal water recycling treatment processes, *Water Res.* **2010**, *44*, 4295-4323, DOI: 10.1016/j.watres.2010.06.020.

[14] Zhang, C.; Cui, S.; Wang, Y., Adsorption removal of pefloxacin from water by halloysite nanotubes. *J. Ind. Eng. Chem.* **2015**, *23*, 12-15, DOI: 10.1016/j.jiec.2014.08.005.

[15] Chowdhury, S.; Sikder, J.; Mandal, T.; Halder, G., Comprehensive analysis on sorptive uptake of enrofloxacin by activated carbon derived from industrial paper sludge. *Sci. Total Environ.* **2019**, *665*, 438-452, DOI: 10.1016/j.scitotenv.2019.02.081.

[16] Otker, H. M.; Akmehmet-Balcioglu, I., Adsorption and degradation of enrofloxacin, a veterinary antibiotic on natural zeolite. *J. Hazard. Mater.* **2005**, *122*, 251-258, DOI: 10.1016/j.jhazmat.2005.03.005.

[17] Anirudhan, T. S.; Shainy, F.; Christa, J., Synthesis and characterization of polyacrylic acid- grafted-carboxylic graphene/titanium nanotube composite for the effective removal of enrofloxacin from aqueous solutions: Adsorption and photocatalytic degradation studies. *J. Hazard. Mater.,* **2017**, *324*, 117-130, DOI: 10.1016/j.jhazmat.2016.09.073.

[18] Perez-Page, M.; Yu, E.; Li, J.; Rahman, M.; Dryden, D. M.; Vidu, R.; Stroeve, P., Template-based syntheses for shape controlled nanostructures. *Adv. Colloid Interface Sci.* **2016**, *234*, 51-79, DOI: 10.1016/

j.cis.2016.04.001.

[19] Ebrahiminezhad, A.; Zare-Hoseinabadi, A.; Sarmah, A. K.; Taghizadeh, S.; Ghasemi, Y.; Berenjian, A., Plant-mediated synthesis and applications of iron nanoparticles. *Mol. Biotechnol.* **2018**, *60*, 154-168, DOI: 10.1007/s12033-017-0053-4.

[20] Shankar, S. S.; Rai, A.; Ahmad, A.; Sastry, M., Rapid synthesis of Au, Ag, and bimetallic Au core-Ag shell nanoparticles using Neem (Azadirachta indica) leaf broth. *J. Colloid Interface Sci.* **2004**, *275*, 496-502, DOI: 10.1016/j.jcis.2004.03.003.

[21] Panigrahi, S.; Kundu, S.; Ghosh, S. K.; Nath, S; Pal, T., General method of synthesis for metal nanoparticles. *J. Nanopart. Res.* **2004**, *6*, 411-414, DOI: 10.1007/s11051-004-6575-2.

[22] Kasthuri, J.; Veerapandian, S.; Rajendiran, N., Biological synthesis of silver and gold nanoparticles using apiin as reducing agent. *Colloid Surf. B-Biointerfaces*. **2009**, *68*, 55-60, DOI: 10.1016/j.colsurfb.2008.09.021.

[23] Zayed, M. F.; Eisa, W. H.; Shabaka, A. A., Malva parviflora extract assisted green synthesis of silver nanoparticles. *Spectroc. Acta Pt. A-Molec. Biomolec. Spectr.* **2012**, *98*, 423-428, DOI: 10.1016/j.saa.2012.08.072.

[24] Makarov, V. V.; Makarova, S. S.; Love, A. J.; Sinitsyna, O. V.; Dudnik, A. O.; Yaminsky, I. V.; Taliansky, M. E.; Kalinina, N. O., Biosynthesis of stable iron oxide nanoparticles in aqueous extracts of hordeum vulgare and rumex acetosa plants. *Langmuir* **2014**, *30*, 5982-5988, DOI: 10.1021/la5011924.

[25] Zhang, P.; Hou, D.; O'Connor, D.; Li, X.; Pehkonen, S.; Varma, R. S.; Wang, X., Green and size-specific synthesis of stable Fe-Cu oxides as earth-abundant adsorbents for malachite green removal. *ACS Sustain. Chem. Eng.* **2018**, *6*, 9229-9236, DOI: 10.1021/acssuschemeng.8b01547.

[26] Rajender, S. V., Greener approach to nanomaterials and their sustainable applications. Curr. *Opin. Chem. Eng.* **2012**, *1*, 123-128, DOI: 10.1016/j.coche.2011.12.002.

[27] Cheng, M.; Wang, Z.; Lv, Q.; Li, C.; Sun, S.; Hu, S., Preparation of amino-functionalized Fe_3O_4@mSiO_2 core-shell magnetic nanoparticles and their application for aqueous Fe^{3+} removal. *J. Hazard. Mater.* **2018**, *341*, 198-206, DOI: 10.1016/j.jhazmat.2017.07.062.

[28] Luo, F.; Yang, D.; Chen, Z.; Megharaj, M.; Naidu, R., The mechanism for degrading orange II based on adsorption and reduction by ion-based nanoparticles synthesized by grape leaf extract. *J. Hazard. Mater.* **2015**, *296*, 37-45, DOI: 10.1016/j.jhazmat.2015.04.027.

[29] Weng, X.; Guo, M.; Luo, F.; Chen, Z., One-step green synthesis of bimetallic Fe/Ni nanoparticles by eucalyptus leaf extract: Biomolecules identification, characterization and catalytic activity. *Chem. Eng. J.* **2017**, *308*, 904-911, DOI: 10.1016/j.cej.2016.09.134.

[30] Wang, X.; Zhan, C.; Ding, Y.; Ding, B.; Xu, Y.; Liu, S.; Dong, H., Dual-core Fe_2O_3@carbon structure derived from hydrothermal carbonization of chitosan as a highly efficient material for selective adsorption. *ACS Sustain. Chem. Eng.* **2017**, *5*, 1457-1467, DOI: 10.1021/acssuschemeng.6b02034.

[31] Tahir, D.; Tougaard, S., Electronic and optical properties of Cu, CuO and Cu_2O studied by electron spectroscopy. *J. Phys. Condes. Matter.* **2012**, *24*, 175002, DOI: 10.1088/0953-8984/24/17/175002.

[32] Zhao, B.; Xu, X.; Zeng, F.; Li, H.; Chen, X., The hierarchical porous structure bio-char assessments produced by co-pyrolysis of municipal sewage sludge and hazelnut shell and Cu(II) adsorption kinetics. *Environ. Sci. Pollut. Res.* **2018**, *25*, 19423-19435, DOI: 10.1007/s11356-018-2079-y.

[33] Yakout, S. M.; Hassan, M. R.; Abdeltawab, A. A.; Aly, M. I., Sono-sorption efficiencies and equilibrium removal of triphenylmethane (crystal violet) dye from aqueous solution by activated charcoal. *J. Clean Prod.* **2019**, *234*, 124-131, DOI: 10.1016/j.jclepro.2019.06.164.

[34] Yadav, M.; Mu, S.; Hyun, J.; Kim, J., Synthesis and characterization of iron oxide/cellulose nanocomposite film. *Int. J. Biol. Macromol.* **2015**, *74*, 142-149, DOI: 10.1016/j.ijbiomac.2014.11.042.

[35] Gupta, S. S.; Bhattacharyya, K. G., Kinetics of adsorption of metal ions on inorganic materials: A review. *Adv. Colloid Interface Sci.* **2011**, *162*, 39-58, DOI: 10.1016/j.cis.2010.12.004.

[36] Hu, X.; Jia, L.; Cheng, J.; Sun, Z., Magnetic ordered

mesoporous carbon materials for adsorption of minocycline from aqueous solution: Preparation, characterization and adsorption mechanism. *J. Hazard. Mater.* **2019**, *362*, 1-8, DOI: 10.1016/j.jhazmat.2018.09.003.

[37] Slimani, R.; El Ouahabi, I.; Abidi, F.; El Haddad, M.; Regti, A.; Laamari, M. R.; El Antri, S.; Lazar, S., Calcined eggshells as a new biosorbent to remove basic dye from aqueous solutions: Thermodynamics, kinetics, isotherms and error analysis. *J. Taiwan Inst. Chem. Eng.* **2014**, *45*, 1578-1587, DOI: 10.1016/j.jtice.2013.10.009.

[38] Zhang, B.; Han, X.; Gu, P.; Fang, S.; Bai, J., Response surface methodology approach for optimization of ciprofloxacin adsorption using activated carbon derived from the residue of desilicated rice husk. *J. Mol. Liq.* **2017**, *238*, 316-325, DOI: 10.1016/j.molliq.2017.04.022.

[39] Zhao, H.; Liu, X.; Cao, Z.; Zhan, Y.; Shi, X.; Yang, Y.; Zhou, J.; Xu, J., Adsorption behavior and mechanism of chloramphenicols, sulfonamides, and non-antibiotic pharmaceuticals on multi-walled carbon nanotubes. *J. Hazard. Mater.* **2016**, *310*, 235-245, DOI: 10.1016/j.jhazmat.2016.02.045.

[40] Yang, W.; Lu, Y.; Zheng, F.; Xue, X.; Li, N.; Liu, D., Adsorption behavior and mechanisms of norfloxacin onto porous resins and carbon nanotube. *Chem. Eng. J.* **2012**, *179*, 112-118, DOI: 10.1016/j.cej.2011.10.068.

[41] Zhou, T.; Fang, L.; Wang, X.; Han, M.; Zhang, S.; Han, R., Adsorption of the herbicide 2,4-dichlorophenoxyacetic acid by Fe-crosslinked chitosan complex in batch mode. *Desalin. Water Treat.* **2017**, *70*, 294-301, DOI: 10.5004/dwt.2017.20508.

[42] Foo, K. Y.; Hameed, B. H., Insights into the modeling of adsorption isotherm systems. *Chem. Eng. J.* **2010**, *156*, 2-10, DOI: 10.1016/j.cej.2009.09.013.

[43] Rivagli, E; Pastorello, A; Sturini, M; Maraschi, F; Speltini, A; Zampori, L; Setti, M; Malavasi, L; Profumo, A., Clay minerals for adsorption of veterinary FQs: Behavior and modeling. *J. Environ. Chem. Eng.* **2014**, *2*, 738-744, DOI: 10.1016/j.jece.2013.11.017.

[44] Sayen, S.; Ortenbach-Lopez, M.; Guillon, E., Sorptive removal of enrofloxacin antibiotic from aqueous solution using a ligno-cellulosic substrate from wheat bran. *J. Environ. Chem. Eng.* **2018**, *6*, 5820-5829, DOI: 10.1016/j.jece.2018.08.012.

[45] Nanta, P.; Kasemwong, K.; Skolpap, W., Isotherm and kinetic modeling on superparamagnetic nanoparticles adsorption of polysaccharide. *J. Environ. Chem. Eng.* **2018**, *6*, 794-802, DOI: 10.1016/j.jece.2017.12.063.

[46] Kumari, M.; Pittman, C. U.; Mohan, D., Heavy metals chromium(VI) and lead(II) removal from water using mesoporous magnetite (Fe_3O_4) nanospheres. *J. Colloid Interface Sci.* **2015**, *442*, 120-132, DOI: 10.1016/j.jcis.2014.09.012.

[47] Li, J.; Cai, J.; Zhong, L.; Cheng, H.; Wang, H.; Ma, Q., Adsorption of reactive red 136 onto chitosan/montmorillonite intercalated composite from aqueous solution. *Appl. Clay Sci.* **2019**, *167*, 9-22, DOI: 10.1016/j.clay.2018.10.003.

[48] Kumar, K. V.; Porkod, K., Relation between some two- and three-parameter isotherm models for the sorption of methylene blue onto lemon peel. *J. Hazard. Mater.* **2006**, *138*, 633-635, DOI: 10.1016/j.jhazmat.2006.06.078.

[49] Loulidi, I.; Boukhlifi, F.; Ouchabi, M.; Amar, A.; Jabri, M.; Kali, A., Kinetic, Isotherm and mechanism investigations of the removal of basic violet 3 from water by raw spent coffee grounds. *Phys. Chem. Res.* **2020**, *57*, 569-584, DOI: 10.22036/pcr.2020.225170.1751.